Linear and Nonlinear Optical Properties of Pyridine−Based Octopolar Chromophores Designed for Chemical Sensing. Joint Spectroscopic and Theoretical Study

ARTICLE *in* THE JOURNAL OF PHYSICAL CHEMISTRY C · DECEMBER 2007

Impact Factor: 4.77 · DOI: 10.1021/jp076066z

Linear and Nonlinear Optical Properties of Pyridine-Based Octopolar Chromophores Designed for Chemical Sensing. Joint Spectroscopic and Theoretical Study

María Moreno Oliva, Juan Casado,*,‡ and Juan T. López Navarrete*,†

Departamento de Química Física, Universidad de Málaga, Campus de Teatinos s/n, Málaga 29071, Spain

Gunther Hennrich

Departamento de Química Orgánica, Universidad Autónoma de Madrid, Cantoblanco, Madrid 28049, Spain

Mari Carmen Ruiz Delgado and Jesús Orduna

Department of Organic Chemistry, ICMA, University of Zaragoza-CSIC, Zaragoza 50009, Spain

Received: July 31, 2007; In Final Form: September 19, 2007

A combined experimental (Raman and electronic spectroscopies) and theoretical (DFT, TD−DFT, and CPHF) study on three octopolar molecules constituted by a central benzene group ramified with acetylene spacers and pyridine groups is presented. Special emphasis is placed on the evolution of the optical properties upon protonation. The Raman and UV−vis spectroscopic properties are related with the nonlinear optical behavior. It is evidenced that the introduction of central methyl groups yields an electron-rich core which thus improves the electronic connection with the external arms through the acetylene spacer. The origin of the β response for the neutral and protonated molecules is rather different: for the former, β results from octopolar contributions (i.e., excited states with trigonal symmetry) while for the latter the increment of β is due to the involvement of dipolar excited states localized in the linear fragments.

I. Introduction

The role in our modern society of telecommunications makes the field of photonics an extremely important area of technological innovation and research. Materials with high nonlinear optical (NLO) activity are very useful as electro-optic switching elements and for optical information processing. In this context, organic molecules appear as promising candidates since they have several advantages over the inorganic NLO homologues: (i) their dielectric constant and refractive index are much smaller, (ii) their polarizabilities are purely electronic, and (iii) they are compatible with the polymer matrix for flexible devices, and so forth.[1−4]

The field of NLO organic molecules is dominated by donor−acceptor substituted asymmetric linear molecules which, however, present important drawbacks such as a high tendency toward unfavorable aggregation, difficult non-centrosymmetric crystallization, and small off-diagonal tensor components.[1−4] After it was recognized that octopolar systems can circumvent these disadvantages, there has been an effort directed toward the synthesis and optimization of their NLO response.[1,4] A common way to design second-order NLO active octopolar molecules is to develop trigonal π-conjugated systems which must display efficient core-to-branches electronic interaction.[4−7] At the molecular level, some key concepts can be explored to learn about the control of the electronic coupling: (i) in the case of **D**onor−**A**cceptor molecules, increasing of the **D**-**A** strength; (ii) conjugation extension from the core to the external arms, and (iii) π-orbital energy matching between the constituting subunits.

Recently, the research in NLO devices has been directed toward functional electro-optical molecules able to act simultaneously as sensing systems.[8] Thus, octopolar dyes must be sensitive to precise electrochemical or chemical inputs such as protons or metal cations upon which the NLO activity should significantly change.[9] The chemical or electrochemical modifications must alter the above cited concepts controlling the NLO activity, and this is the focus of the present paper. We have recently synthesized octopolar chromophores with switchable second-order NLO activity based on different benzene cores trigonally ramified with pyridylethynyl branches (Figure 1).[10] In addition to the different substitution patterns in the central part, the N-center of the pyridyl rings shows different topology regarding the neighbor triple bonds. As can be deduced, this N-center can be protonated and the electronic coupling with the vicinal/distant π-electron network altered for providing potential NLO sensing.

In this paper we propose the study of these molecules in their neutral and fully triprotonated states. We are particularly interested in the analysis of the electronic and molecular structures according to the substitution patterns and in their changes upon protonation. A set of linear spectroscopic techniques (UV−vis absorption and emission) together with Raman spectroscopy are employed and fully supported by density functional theory model calculations. In a further effort, the NLO activity is addressed also theoretically using proper quantum-chemical sources. The paper tries to get precise insights of the molecular features determined by the substitution pattern in connection with the electronic structure (i.e., core-to-branches π-conjugational coupling), determining the linear and nonlinear

* Corresponding authors.
† Telephone: 0034-952132018. Fax: 0034-952132000. E-mail: teodomiro@uma.es.
‡ E-mail: casado@uma.es.

10.1021/jp076066z CCC: $37.00
Published on Web 11/29/2007

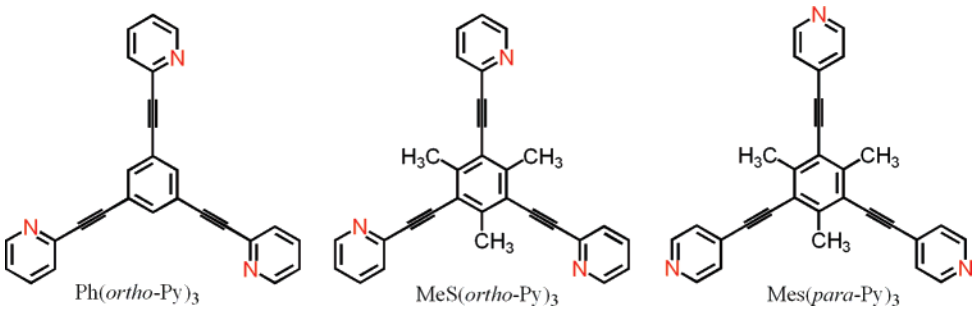

Figure 1. Chemical structures and nomenclatures of the studied compounds. Ph: phenyl; Mes: mesityl; Py: pyridyl.

properties. Finally, the effects of protonation will be related with the optimization of the NLO sensing activity.

II. Experimental and Theoretical Details

The syntheses of all the compounds studied have been reported previously.[10] Protonation was carried out in THF by addition of small amounts of a concentrated aqueous solution of HCl. Absorption and emission spectra were obtained in THF or dichloromethane in concentrations (ca. $10^{-6}-10^{-7}$ M) not exceeding the 0.1 au of absorbance (1 cm path length cell). Under these conditions, the absorption intensity was found to have a linear dependence with concentration. No spectral shifts in the absorption spectra have been observed, indicating the absence of aggregation in the system. UV−vis absorption spectra were recorded on an Agilent 8453 instrument equipped with a diode array detection system. Emission spectra were measured using a JASCO FP-750 spectrofluorometer. No fluorescent contaminants were detected upon excitation in the wavelength region of experimental interest. FT−Raman spectra were measured using an FT−Raman accessory kit (FRA/106−S) of a Bruker Equinox 55 FT−IR interferometer. A continuous-wave Nd−YAG laser working at 1064 nm was employed for excitation. A germanium detector operating at liquid nitrogen temperature was used. Raman scattering radiation was collected in a back-scattering configuration with a standard spectral resolution of 4 cm^{-1}. In order to avoid possible damage to the samples upon laser radiation, its power was kept at a level lower than 20 mW, and 1000−3000 scans were averaged for each spectrum. Raman spectra in solution were obtained in analytical grade CH_2Cl_2 and THF.

Density functional theory methods have become very popular since the inclusion of electron correlation effects with accuracies comparable to those of correlated ab initio procedures, such as MP2, while reducing substantially the computational costs of the latter.[11] Hence, ground-state total energies, equilibrium geometries, eigenfrequencies, and normal coordinates were calculated using density functional theory by means of the Gaussian-03 package of programs.[12] The Becke's three-parameter (B3) gradient-corrected exchange functional combined with the correlation Lee−Yang−Parr (LYP) functional was utilized.[13] The 6-31G** basis set was used.[14] In order to reduce the computational treatment, nonplanar symmetries with a C_3 axis are initially considered. However, upon energy optimization, the ground electronic state of molecules adopts planar conformations (C_{3v} for Mes(*para*-Py)$_3$, C_{3h} for Ph(*ortho*-Py)$_3$, and C_3 for Mes(*ortho*-Py)$_3$). In order to check if this planarization is an artifact, some of the properties are recalculated for forced nonplanar geometries (i.e., only with a C_3 axis) obtaining essentially the same results. This is reasonable since the introduction of acetylene spacers between the core and the outer groups is exploited because of the reduced steric core-to-branch crowding, and hence minimal distortions, allowing a reasonably good electronic communication. Theoretical Raman spectra were obtained for the resulting ground-state optimized geometries, harmonic vibrational frequencies and Raman intensities were calculated numerically. In order to improve the experimental-to-theoretical comparison, theoretical frequencies are uniformly scaled down by a random factor (0.96) which are thus the reported values.[15]

The time-dependent DFT (TD−DFT) approach is now being widely applied in both chemistry and condensed matter physics to describe electronic excitations.[16] While it is not as accurate for excitations as the ordinary DFT is for ground-state properties, this theory has a considerable predictive power and is computationally quite tractable. At least thirty lowest-energy electronic excited states were computed for all the molecules. TD−DFT calculations were performed using the same functional (B3LYP) and basis set (6-31G**). Relative to NLO calculations, excited-state dipole moments were calculated using the RHOCI density on the previously optimized molecular geometries. Molecular orbital contours were plotted by using Molekel 4.3.[17] The tensor components of the static first hyperpolarizability have been analytically calculated by using the coupled perturbed Hartree−Fock (CPHF) method.[18,19]

III. Electronic Structure

III.1. Non-protonated Molecules. Effect of CH_3-Core and *N*-Pyridyl Substitution. Figure 2 shows the UV−vis absorption and emission spectra of the compounds, whereas Figure 3 represents the absolute theoretical energies of the orbitals around the gap.

The most intense absorption contains vibronic structure (i.e, in Mes(*ortho*-Py)$_3$ subpeaks are spaced by 1700−1000 cm^{-1}). The lowest-energy vibronic peak of the progression moves to 308 nm in Ph(*ortho*-Py)$_3$, 315 nm in Mes(*ortho*-Py)$_3$, and 313 nm in Mes(*para*-Py)$_3$ and similarly the strongest vibronic peak. This experimental band can be related with the superposition of the degenerated $S_0 \rightarrow S_2$ and $S_0 \rightarrow S_3$ TD−DFT excitations which are predicted at 317 nm in Ph(*ortho*-Py)$_3$, 326 nm in Mes(*ortho*-Py)$_3$, and 322 nm in Mes(*para*-Py)$_3$, composed of the following one-electron excitations: $S_0 \rightarrow S_2$ [HOMO-1→LUMO + HOMO→LUMO+1] and $S_0 \rightarrow S_3$ [HOMO-1→LUMO+1 + HOMO→LUMO]. In the high-energy side of this band, around 260−270 nm, a new band is detected which relates with an overlap of nearly degenerated theoretical excitations (i.e., $S_0 \rightarrow S_5$ + $S_0 \rightarrow S_6$ + $S_0 \rightarrow S_7$ + $S_0 \rightarrow S_8$) between 285 and 295 nm. The $S_0 \rightarrow S_1$ excitation is predicted around 350 nm and is ascribed to the weak experimental bands measured almost 30 nm at higher energies relative to the strongest peak. This theoretical excitation corresponds, however, to a prohibited excitation and the observation would be caused by some planar distortion in solution. Emission spectra and fluorescence quantum yields of the two mesityl derivatives are very similar showing the preponderance of the core in the emissive state which further-

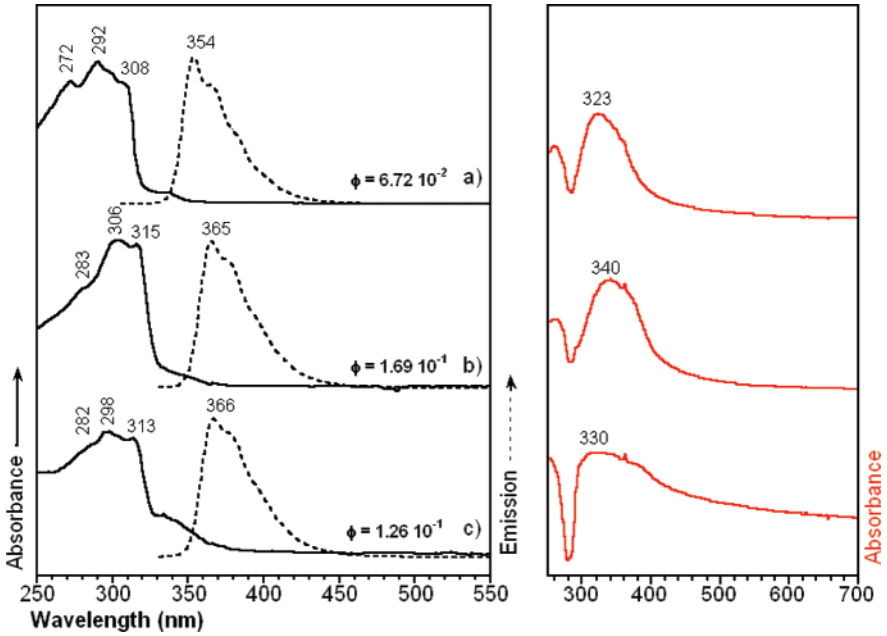

Figure 2. UV−vis absorption and emission spectra in dichloromethane and THF, respectively, for (a) Ph(*ortho*-Py)$_3$, (b) Mes(*ortho*-Py)$_3$, and (c) Mes(*para*-Py)$_3$. Spectra in red correspond to the triprotonated species.

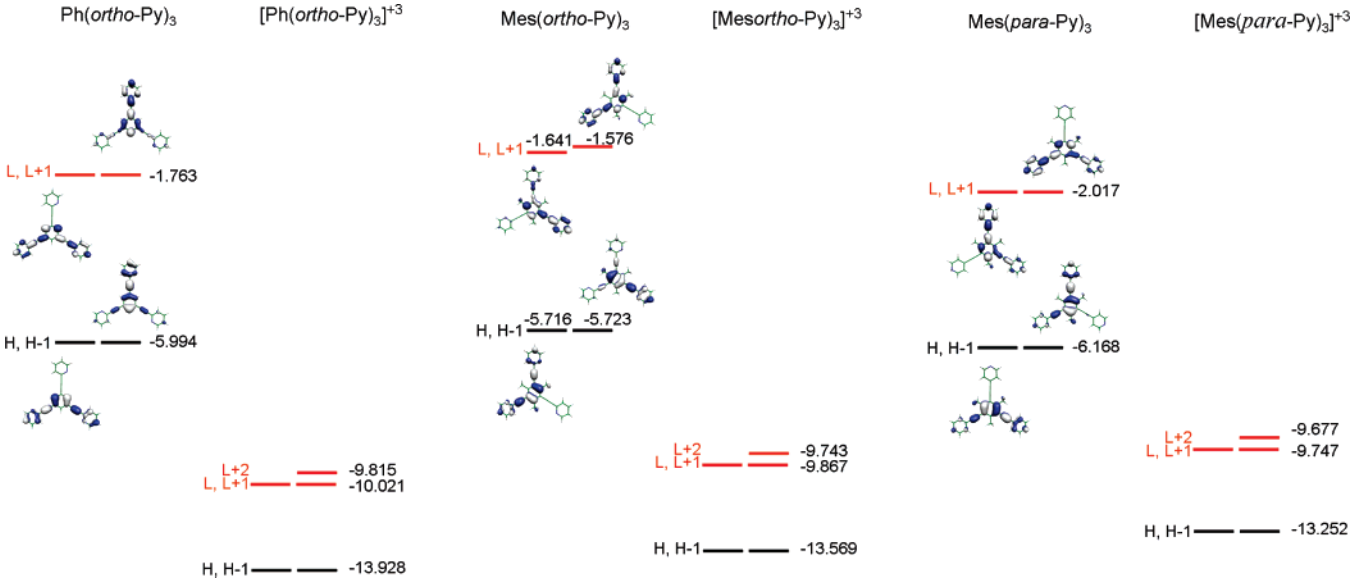

Figure 3. DFT/B3LYP/6-31G** energy and topologies for the orbitals around the gap for the neutral and triprotonated samples.

more induces an increment of the fluorescence intensity by one order of magnitude.

The HOMO and HOMO-1, as well as the LUMO and LUMO+1, are energy-degenerated orbitals for all octopolar compounds. Upon inclusion of the methyl groups on Mes(*ortho*-Py)$_3$, the contribution (i.e., hyperconjugation) of the CH methyl bonds (see orbital topologies) pushes up more effectively the HOMO and HOMO-1 than the LUMO and LUMO+1 which produces an energy gap reduction with respect to Ph(*ortho*-Py)$_3$. From Mes(*ortho*-Py)$_3$ to Mes(*para*-Py)$_3$ there is an enlargement of the energy gap due to the stabilization of the frontier orbitals, an effect more accentuated for the occupied terms. It is noticeable that in Mes(*para*-Py)$_3$ the HOMO-1 and HOMO have similar wavefunctions (i.e., with the only difference being the above-described C−H bonds effect), in contrast to the case of Mes(*ortho*-Py)$_3$ where the HOMO-1 and HOMO orbitals spread over two and one arms, respectively. This description means that the nitrogen-*pz* atomic orbital plays a role as for the whole trigonal π-network and is not only restricted to the pyridyl unit. Electrochemical data could provide some insights on these effects but were inaccessible by cyclic voltammetry. Instead, Raman spectra in the next sections will show interesting wavenumber differences probably residing in these changes in the electronic structure.

III.2. Effect of Protonation and the Appearance of Charge-Transfer States. The spectra of the protonated species are characterized by one broad band (i.e., 300−500 nm), less intense than the homologue in the neutral samples. This absorption appears at 323 nm (i.e., TD−DFT at 348 nm) in Ph(*ortho*-Py)$_3$, 340 nm (i.e., TD−DFT at 369 nm) in Mes(*ortho*-Py)$_3$, and 330 nm (i.e., TD−DFT at 386 nm) in Mes(*para*-Py)$_3$. This band involves several excitations which furthermore change their composition in the series. For example, for Mes(*para*-Py)$_3$ the band corresponds to the energy-degenerated $S_0 \rightarrow S_4$ and $S_0 \rightarrow S_5$ excitations mainly composed by the HOMO→LUMO+2 the $S_0 \rightarrow S_4$ and the HOMO-1→LUMO+2 the $S_0 \rightarrow S_5$. Moreover,

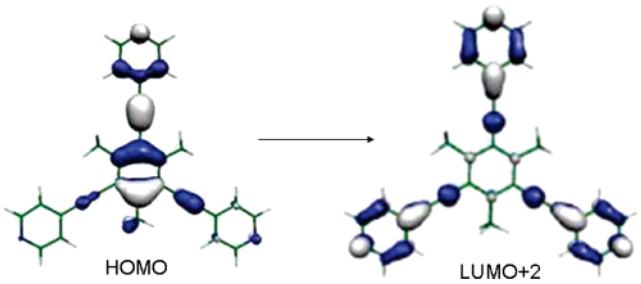

Figure 4. Orbital topologies for $[Mes(para\text{-}Py)_3]^{3+}$.

it is noticed that each excitation is composed for an increasing number of one-electron transitions revealing the orbital mixing likely due to electron correlation, a phenomena which did not occur in the neutral molecules. Quantum chemical calculations predict the narrowing of the energy gap upon protonation (see Figure 3).

As a distinctive feature of the charged species regarding the neutral analogues, there exists an important contribution of the LUMO+2 orbital (see Figure 4) to the transitions involved in the strongest UV−vis absorption band, a fact that does not take place in the neutral case for which the LUMO+2 is missing among the relevant terms. This orbital shows a net charge density concentration in the pyridyl moieties relative to the mesityl core. This means that the HOMO→LUMO+2 transition can be understood as an electron reorganization from the center of the molecule (i.e., HOMO and HOMO-1) to the external branches thus reflecting a certain degree of electron charge transfer. This description is relevant due to its incidence in the NLO response, especially sensitive to the appearance of charge transfer, and consequently in the change of the NLO values from the neutral compounds (i.e., charge-transfer processes are absent) to the chemically treated samples.

IV. Molecular Structure

IV.1. Non-protonated Molecules. Effect of CH_3-Core and *N*-Pyridyl Substitution. Figure 5 shows the FT-Raman spectra of the neutral and protonated compounds, while Figure 6 summarizes the main geometrical parameters (i.e., bond lengths) of the optimized geometries obtained theoretically.

The Raman spectra of the neutral compounds show a very intense Raman line around 2220 cm^{-1} due to the symmetric in-phase stretching mode of the acetylene spacers. The frequency of this band slightly moves down upon substitution of the central core and after *ortho*→*para* change on the pyridyl group which is in agreement with the slight and continuous lengthening of the triple bond (Figure 6). In a previous work on C_3 molecules with a donor−acceptor substitution pattern, we have found a relationship between the frequency downshift of this ν(C≡C) and π-electron delocalization along the acetylene spacers, hence the −3 cm^{-1} displacement of this triple-bond frequency might indicate an electronic coupling between the pyridyl unit and the triple bonds.[9] Figures S1 and S2 of Supporting Information display the DFT/B3LYP/6-31G** theoretical Raman spectra of the three samples as well as the corresponding vibrational normal modes associated with the bands discussed in the text.

The band at 1578 cm^{-1} in Ph(*ortho*-Py)$_3$ consists of a ring stretching mode of the pyridyl group where the parallel CC and CN bonds display the greatest motion amplitudes. This line shifts to 1582 cm^{-1} upon methyl substitution of the central core in Mes(*ortho*-Py)$_3$. An analogue vibrational mode that now involves the CC bonds parallel to the acetylene is measured at 1594 cm^{-1} in the *para*-isomer (this based on theory, the origin of the +4 cm^{-1} shift (1578 cm^{-1}→1582 cm^{-1}) is unclear since theoretical bond distances and Raman frequencies remain almost constant for this bond and mode. The bands at 1560 and 1557 cm^{-1} in Mes(*ortho*-Py)$_3$ and Mes(*para*-Py)$_3$, respectively [i.e., absent in Ph(*ortho*-Py)$_3$], correspond to ring CC stretches of the central hexa-substituted core. In the medium-energy region of the vibrational spectra of the neutral species, medium intense Raman bands are observed at almost the same frequency in the *ortho*-derivatives, 1190 cm^{-1} in Ph(*ortho*-Py)$_3$, and 1191 cm^{-1} in Mes(*ortho*-Py)$_3$, but moves to 1174 cm^{-1} in the *para*-isomer. According to calculations, this band is mostly described as a deformation mode of the core ring which is particularly coupled with the stretching modes of the entire C−C≡C−C spacer (see

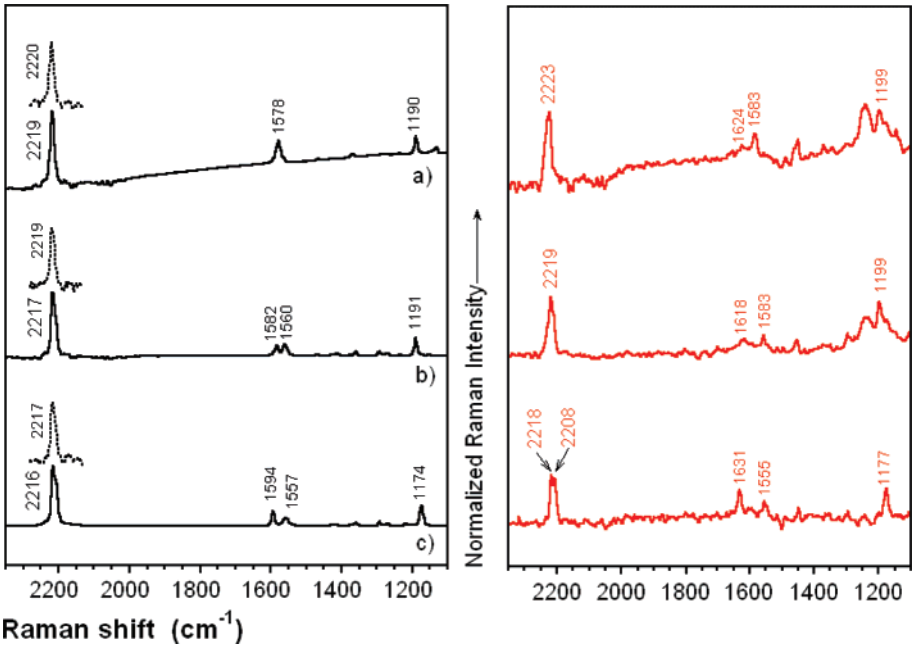

Figure 5. FT-Raman spectra in the solid state for (a) Ph(*ortho*-Py)$_3$, (b) Mes(*ortho*-Py)$_3$, and (c) Mes(*para*-Py)$_3$. Spectra in red correspond to the triprotonated species. Dashed lines correspond to the spectra in solution.

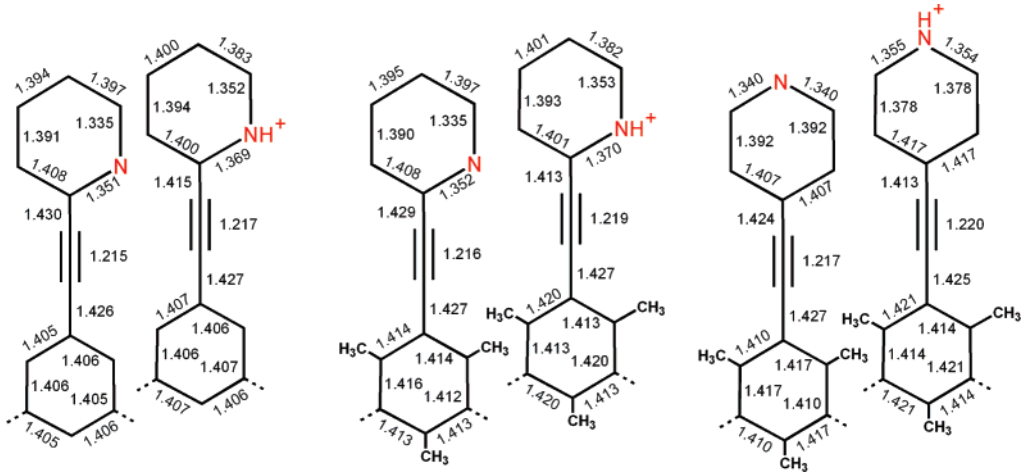

Figure 6. DFT/B3LYP/6-31G** optimized geometries for the neutral and triprotonated compounds.

TABLE 1: First Hyperpolarizabilities of Octopolar 1,3,5-Trisalkynylbenzene Derivatives[a]

β-values	Ph(*ortho*-P y)$_3$	Mes(*ortho*-P y)$_3$	Mes(*para*-P y)$_3$	[Ph(*ortho*-Py)$_3$]$^{3+}$	[Mes(*ortho*-P y)$_3$]$^{3+}$	[Mes(*para*-Py)$_3$]$^{3+}$
β_{xxx0}[b]	8 ± 1	9 ± 1	12 ± 3	19 ± 3	38 ± 2	146 ± 5
β_{xxx}[c]	3.606	10.368	11.634	15.929	26.305	45.340

[a] All of the values are given in 10−30 esu. [b] Static hyperpolarizability, HRS data obtained in THF−HCl_{aq} from ref 10. [c] Theoretical data calculated by the CPHF method using the 6-31G** basis set on DFT//B3LYP/6-31G** optimized geometries.

TABLE 2: Results of TD-B3LYP/6-31G Calculations on the Neutral Compound Mes(*para*-Py)$_3$**

molecules	E_{max} (eV)	f_{osc}[a]	major contributions[b]	$\|\mu_{12}\|$(*D*)	$\|\Delta\mu_{12}\|$(*D*)
Mes(*para*-Py)$_3$	3.85	1.05	H-1→L+1 (42%) H→L (42%)	8.34	0.99
	3.85	1.05	H-1→L (42%) H→L+1 (−42%)	8.34	0.99
	4.15	0.21	H→L+2 (91%)	3.57	8.24
	4.15	0.21	H-1→L+2 (91%)	3.57	8.24
	4.42	0.22	H-2→L (90%)	3.64	8.52
	4.42	0.22	H-2→L+1 (90%)	3.64	8.52

[a] Only transitions with $f_{osc} > 0.10$ are included. [b] H = HOMO, L = LUMO; only contributions above 20% are included.

Figure S2 of Supporting Information) which explains the observed frequency displacement.

IV.2. Effect of Protonation. There exists a small change in the triple-bond stretching frequency upon protonation which might be related with the also small change on the C≡C bond lengths (i.e., +0.002−0.003 Å) after positive charging. Within the protonated molecules, this frequency varies as in the case of the neutral molecules.

The Raman bands at 1624 cm^{-1} in [Ph(*ortho*-Py)$_3$]$^{3+}$, at 1618 cm^{-1} in Mes(*ortho*-Py)$_3$, and at 1631 cm^{-1} in Mes(*para*-Py)$_3$ are new features resulting from protonation. In order to attribute a physical meaning to this band we have obtained the theoretical Raman spectrum of [Ph(*ortho*-Py)$_3$]$^{3+}$ which reproduces the appearance of a new band at 1594 cm^{-1} probably corresponding to the experimental 1624 cm^{-1} line. This band is described as a ν(CC)+ν(CN) ring mode whose dynamics is close to that associated with the neutral line at 1578 cm^{-1}. Despite the above simple description of this mode in terms of two internal coordinates, its ring character must be emphasized and hence its displacement by +46 cm^{-1} is ascribable to the strengthening of the CC bonds in the pyridyl ring upon protonation and ring de-aromatization.

V. Nonlinear Optical Properties

V.1. Non-protonated Molecules. Effect of CH_3-Core and *N*-Pyridyl Substitution. The nonlinear optical response of octopolar 1,3,5-trisalkynylbenzenes was measured by the hyper-Rayleigh scattering (HRS) method.[10] The tensor components of the static first hyperpolarizability have been also calculated by the CPHF method on the resulting B3LYP/6-31G** ground-state optimized geometries restricted to C_{3h} symmetry. Comparing the β-values listed in Table 1, both experimental and theoretical data are in excellent agreement, taking into account that the β-values have been calculated on the lowest energy conformations in vacuum, while experimental data were obtained in solution.

The central benzene ring is electron-rich and may act as a donor relative to the peripheral *sp* hybridized C≡C carbon atoms; thus, the inclusion of hyperconjugating donor substituents (−CH_3) should result in more favorable core-to-branches charge transfer which in turn should lead to enhanced β-values. This suggestion is experimentally and theoretically supported in Table 1 for the β-values on passing from Ph(*ortho*-Py)$_3$ to the mesityl derivatives and is also in agreement with the evolution of the energy gap. For Mes(*ortho*-Py)$_3$ and Mes(*para*-Py)$_3$ the data are quite similar (see experiments within the error bars). An opposite behavior of energy and optical gaps and β-values is found for the mesityl derivatives. However, the NLO results agree with the continuous downshift displacement of the ν(C≡C) Raman band. This Raman behavior is consistent with an increment of π-electron delocalization between the core and the arms which leads to the enhancement of the NLO response. Therefore β/Raman frequencies increase/decrease such as Ph(*ortho*-Py)$_3$→Mes(*ortho*-Py)$_3$→Mes(*para*-Py)$_3$.

TABLE 3: Results of TD-DFT/B3LYP/6-31G Calculations on the Triprotonated Octopolar Forms**

molecules	E_{max} (eV)	f_{osc}[a]	major contributions[b]	$\|\mu_{12}\|$(D)	$\|\Delta\mu_{12}\|$ (D)
[Ph(*ortho*-Py)$_3$]$^{3+}$	3.56	1.01	H-1→L (21%) H-1→L+1 (20%) H→L (20%) H→L+1 (−21%)	6.95	3.86
	3.56	1.01	H-1→L (−20%) H-1→L+1 (21%) H→L (21%) H→L+1 (20%)	6.95	3.86
	3.71	0.13	H→L+2 (87%)	2.96	12.47
	3.71	0.13	H-1→L+2 (87%)	2.96	12.47
	4.10	0.25	H-2→L (91%)	3.65	11.72
	4.10	0.25	H-2→L+1 (91%)	3.65	11.72
[Mes(*ortho*-Py)$_3$]$^{3+}$	3.36	0.97	H-1→L (30%) H→L+1 (−30%)	8.45	4.92
	3.36	0.97	H-1→L+1 (30%) H→L (30%)	8.45	4.92
	3.42	0.15	H→L+2 (88%)	2.92	11.73
	3.42	0.15	H-1→L+2 (88%)	2.92	11.73
	4.13	0.24	H-2→L (75%)	3.45	11.10
	4.13	0.24	H-2→L+1 (75%)	3.45	11.10
	4.37	0.19	H-1→L+4 (36%) H→L+3 (36%)	2.60	9.42
	4.37	0.19	H-1→L+3 (36%) H→L+4 (−36%)	2.60	9.42
[Mes(*para*-Py)$_3$]$^{3+}$	3.21	1.07	H→L+2 (56%)	9.21	9.15
	3.21	1.07	H-1→L+2 (56%)	9.21	9.15
	4.08	0.24	H-2→L+1 (85%)	3.71	11.32
	4.08	0.24	H-2→L+1 (85%)	3.71	11.32

[a] Only transitions with $f_{osc} > 0.10$ are included. [b] H = HOMO, L = LUMO; only contributions above 20% are included.

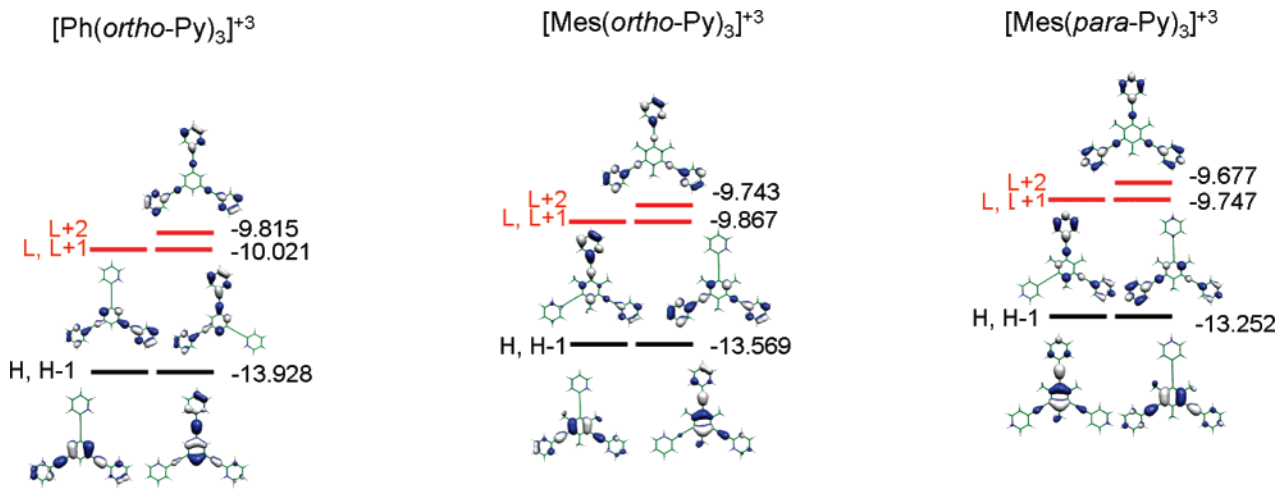

Figure 7. DFT/B3LYP/6-31G** energy and topologies for the orbitals around the gap for the triprotonated samples.

As discussed above, the analysis of DFT molecular orbitals (MO diagram) reveals the presence of pairs of degenerate orbitals which do not display an octopolar symmetry (i.e., C_{3h}) and can therefore give rise to localized excited states,[20−22] whereas the nondegenerate orbitals (i.e., LUMO+2) display a C_{3h} symmetry (see Figures 3 and 4). The existence of excited states with nonzero dipole moment has been explored by using TD−DFT calculations, and the results for compound Mes(*para*-Py)$_3$, taken as a prototype, are reported in Table 2. The degenerate excited states with nonzero dipole moment are associated with the highest-energy degenerate electronic transitions calculated at 4.15 eV ($f = 0.21$) and 4.42 eV ($f = 0.22$), whereas those associated with the lowest-energy degenerate electronic transitions calculated at 3.85 eV ($f = 1.05$) have a small dipole moment change (0.99 D). In other words, the quadratic NLO response of the neutral octopolar trisalkynylbenzenes are associated with electronic transitions to octopolar excited states which depend on the transition dipole moment between excited states, quantities which are not accessible via the TD−DFT modeling approach.

IV.2. Effect of Protonation. Protonated 1,3,5-trisalkynylbenzene derivates exhibit high β-values (see Table 1). For instance, the increase of the dynamic hyperpolarizability $\beta_{xxx,800}$ amounts to a factor of 17 for Mes(*para*-Py)$_3$ upon protonation (i.e., from 37×10^{-30} esu for Mes(*para*-Py)$_3$ to 623×10^{-30} esu for the threefold protonated [Mes(*para*-Py)$_3$]$^{3+}$, see ref 9). It must be also stressed that the order of β increase for the triply-charged compounds is the same as that for the neutral structures: [Mes(*para*-Py)$_3$]$^{3+}$ > [Mes(*ortho*-Py)$_3$]$^{3+}$ > [Ph(*ortho*-Py)$_3$]$^{3+}$. Theoretical CPHF data also reproduce, in good accordance, this experimental trend.

In contrast to that observed for the neutral compounds, upon generation of the triply-charged compound [Mes(*para*-Py)$_3$]$^{3+}$, it is predicted that there will be a large dipole moment change, which amounts to 9.15 D, associated with the lowest-energy degenerate electronic transitions calculated at 3.21 eV and

composed by HOMO→LUMO+2 and HOMO-1→LUMO+2 (Table 3). The pronounced charge-transfer character (see Figure 7) of these transitions along with their large oscillator strength ($f = 1.07$) accounts for a large contribution to the overall molecular hyperpolarizability.

This result thus confirms the existence of several pairs of degenerated excited states with nonzero dipole moments in the triply charged compound $[Mes(para\text{-}Py)_3]^{3+}$ that are responsible for the dipolar contribution to the molecular first hyperpolarizability. However, according to the results shown in Table 3, the dipole moment change associated with the lowest-energy degenerate electronic transitions in $[Ph(ortho\text{-}Py)_3]^{3+}$ and $[Mes(ortho\text{-}Py)_3]^{3+}$ is less pronounced than that calculated for $[Mes(para\text{-}Py)_3]^{3+}$. Thus, very probably, dipolar contributions to the second-order NLO activity can be triggered by protonation and further tuned by inclusion of methyl groups into the benzene core and upon *ortho*→*para* change on the pyridyl group. Overall, these data are related with the observation, at the lowest Raman frequency among the protonated derivatives, of the ν(C≡C) Raman band in $[Mes(para\text{-}Py)_3]^{3+}$ likely supporting its high NLO activity. As already explained for the neutral compounds, in this case as well, there is not a straightforward relationship between optical gaps and NLO response; nevertheless, β-values increase as the HOMO−LUMO energy gap (ΔE) decreases (i.e., as the donor strength of the core increases and as the degree of conjugation with the periphery is enhanced).

VI. Conclusions

A combined experimental (Raman and electronic spectroscopies) and theoretical (DFT, TD−DFT, and CPHF) study on three trigonal octopolar molecules constituted by a central benzene and mesityl core ramified with acetylene spacers and pyridine groups is presented. Motivated by the utility of these compounds in chemical (i.e., proton) sensing, special attention is paid to the evolution of the properties upon protonation. The experimental work analyzes the electronic absorption, fluorescence, and Raman spectra while the theoretical part supports all the experimental properties. A complementary study and comprehensive understanding of the NLO properties is provided in relation to the Raman and UV−vis data. The strongest Raman band, due to the ν(C≡C) stretching modes, and β show a common behavior ascribed to the increment of π-electron delocalization which is optimal among the samples for $Mes(para\text{-}Py)_3$. The introduction of methyl groups yields a better electron donor core which thus improves the electronic connection with the external arms through the acetylene spacer. To support this, precise electronic and structural data are described. Interestingly, the origin of the β response has been outlined which results, for the neutral systems, from octopolar contributions (i.e., excited states with zero dipole moment change), while the significant increment of β after protonation is due to the involvement of dipolar excited states yielding dipolar contributions to the NLO outcome. As a result, this paper provides evidence that the NLO activity in these samples can be accordingly enhanced by inclusion of donor→acceptor interactions. In this regard, Raman spectroscopy combined with electronic structure calculations can be used to quickly evaluate the potentiality of a given compound for organic applications.

Acknowledgment. The present work was supported in part by the Dirección General de Enseñanza Superior (DGES, MEC, Spain) through Research Project Nos. CTQ2006-14987-C02-01 and CTQ2005-01368. The authors are also indebted to Junta de Andalucía and Gobierno de Aragón (Spain) for funding their research groups FQM-0159 and E39. J.C. is grateful to the MEC of Spain for an I3 professorship position of Chemistry at the University of Málaga. M.M.O. and M.C.R.D. acknowledge the MEC for a FPU grant and MEC/Fulbright Postdoctoral Fellowship at the Georgia Institute of Technology, respectively.

Supporting Information Available: Figures S1 and S2 display the DFT/B3LYP/6-31G** theoretical Raman spectra of the three samples as well as the corresponding vibrational normal modes associated with the bands discussed in the text. This material is available free of charge via the Internet at http://pubs.acs.org.

References and Notes

(1) Zyss, J. *Molecular Nonlinear Optics: Materials, Physics and Devices*; Academic Press: New York, 1994. Zyss, J.; Ledoux, I. *Chem. Rev.* **1994**, *94*, 77.

(2) Kanis, D. R.; Ratner, M. A.; Marks, T. J. *Chem. Rev.* **1994**, *94*, 195.

(3) Marder, S. R.; Perry, J. W.; Schaeffer, W. P. *Science* **1989**, *245*, 626. Marder, S. R.; Gorman, C. B.; Meyers, F.; Perry, J. W.; Bourhill, G.; Brédas, J. L.; Pierce, B. M. *Science* **1994**, *265*, 632. Marder, S. R. *Chem. Commun*. **1989**, *2006*, 131.

(4) Clays, K.; Persoons, A. *Phys. Rev. Lett.* **1991**, *66*, 2980. Verbiest, T.; Clays, K.; Samyn, C.; Wolff, J.; Reinhoudt, D.; Persoons, A. *J. Am. Chem. Soc*. **1994**, *116*, 9320. Asselberghs, I.; Clays, K.; Persoons, A.; Ward, M. D.; McCleverty, J. *J. Mater. Chem*. **2004**, *14*, 2831.

(5) Blanchard-Desce, M.; Baudin, J.-B.; Ruel, O.; Jullien, L.; Brasselet, S.; Zyss, J. *J. Opt. Mater*. **1998**, *9*, 276. Greve, D. R.; Schougaard, S. B.; Geisler, T.; Petersen, J. C.; BjØrnholm, T. *Adv. Mater*. **1997**, *9*, 1113. Thalladi, V. R.; Brasselet, S.; Bläser, D.; Boese, R.; Zyss, J.; Nangia, A.; Desiraju, G. R. *Chem. Commun*. **1997**, 1841.

(6) Lee, W. H.; Lee, H.; Kim, J.-A.; Choi, J.-H.; Cho, M.; Jeon, S.-J.; Cho, B. R. *J. Am. Chem. Soc*. **2001**, *123*, 10658.

(7) Moreno Oliva, M.; Casado, J.; Hennrich, G.; López Navarrete, J. T. *J. Phys. Chem. B* **2006**, *110*, 19198.

(8) Feringa, B. L. *Molecular Switches*; Wiley-VCH: Weinheim, 2001.

(9) Pond, S. J. K.; Tsutsumi, O.; Rumi, M.; Kwon, O.; Zojer, E.; Bredas, J. L.; Marder, S. R.; Perry, J. W. *J. Am. Chem. Soc*. **2004**, *126*, 9291. Asselberghs, I.; Zhao, Y.; Clays, K.; Persoons, A.; Comito, A.; Rubin, Y. *Chem. Phys. Lett.* **2002**, *364*, 279.

(10) Asselberghs, I.; Hennrich, G.; Clays, K. *J. Phys. Chem. A* **2006**, *110*, 6271.

(11) Stephens, P. J.; Devlin, F. J.; Chabalowski, F. C. F.; Frisch, M. J. *J. Phys. Chem*. **1994**, *98*, 11623. Novoa, J. J.; Sosa, C. *J. Phys. Chem.* **1995**, *99*, 15837. Casida, E.; Jamorski, C.; Casida, K. C.; Salahub, D. R. *J. Chem. Phys.* **1998**, *108*, 4439. Stratmann, R. E.; Scuseria, G. E.; Frisch, M. J. *J. Chem. Phys.* **1998**, *109*, 8218.

(12) Frisch, M. J., et al. *Gaussian 03*, revision B.05; Gaussian, Inc.: Pittsburgh, PA, 2003.

(13) Becke, A. D. *J. Chem. Phys.* **1993**, *98*, 1372.

(14) Francl, M. M.; Pietro, W. J.; Hehre, W. J.; Binkley, J. S.; Gordon, M. S.; Defrees, D. J.; Pople, J. A. *J. Chem. Phys.* **1982**, *77*, 3654.

(15) Scott, A. P.; Radom, L. *J. Phys. Chem*. **1996**, *100*, 16502.

(16) Runge, E.; Gross, E. K. U. *Phys. Rev. Lett*. **1984**, *52*, 997. Gross, E. K. U.; Kohn, W. *Adv. Quantum Chem*. **1990**, *21*, 255. Gross, E. K. U.; Driezler, R. M. Plenum Press: New York, 1995.

(17) Portmann, S.; Lüthi, H. P. *Chimia* **2000**, *54*, 766.

(18) Pulay, P. *J. Chem. Phys.* **1983**, *78*, 5043.

(19) Dykstra, C. E.; Jasien, P. G. *Chem. Phys. Lett.* **1984**, *109*, 388.

(20) Andraud, C.; Zabulon, T.; Collet, A.; Zyss, *J. Chem. Phys*. **1999**, *245*, 243.

(21) (a) Lee, Y. K.; Jeon, S. J.; Cho, M. *J. Am. Chem. Soc.* **1998**, *120*, 10921. (b) Cho, M.; Kim, H. S.; Jeon, S. J. *Chem. Phys.* **1998**, *108*, 7114.

(22) Coe, B. J.; Harris, J. A.; Brunschwig, B. S.; Asselberghs, I.; Clays, K.; Garín, J.; Orduna, J. *J. Am. Chem. Soc.* **2005**, *127*, 13399−13410. Vance, F. W.; Hupp, J. T. *J. Am. Chem. Soc.* **1999**, *121*, 4047.